Planar Test Objects for Photogrammetric Calibration of Enhanced Vision Systems Cameras: Application Practice

Ivan Kholopov [1], Igor Kudinov [1] and Mikhail Nikiforov [1]

[1] Ryazan State Radio Engineering University named after V.F. Utkin, Gagarina st, 59/1, Ryazan, 390005, Russia

Abstract

Two variants of constructs of planar test objects, which can be used to evaluate the internal and external parameters of video cameras operating as part of an enhanced vision system consisting of several video cameras in the visible and infrared wavelength ranges, are considered: with stationary electric heater and with portable electric heater like dock station. The design of both planar test objects consists of the light planar aluminum plate, squares from dark vinyl film, electric heating element and thermostat. The design of the device for performing automated camera calibration is presented. It is shown that the evaluation of the homography matrix based on the results of the performed preliminary calibration makes it possible to superimpose visible and long wave infrared images with an absolute error of the order of units of pixels.

Keywords

Camera calibration, enhanced vision systems, test object, camera intrinsic and extrinsic parameters, multispectral image superimposition, image fusion.

1. Introduction

Enhanced vision is a technology that incorporates information from different optic sensors to provide vision in limited visibility environments. Aircraft enhanced vision systems (EVS) for increased pilot visibility and flight safety allow to perform different flight operations in darkness, smoke, haze, rain, fog, and other low visibility conditions [1]. In the general case, EVS can contain cameras of the visible and various infrared (IR) ranges – near IR (NIR), short wave IR (SWIR), mid-wave IR (MWIR), and long wave IR (LWIR) – for providing a good situational awareness in different visibility conditions. The use of these ranges is caused by the presence of atmospheric transparency windows with a radiation transmittance of more than 0.5 [2]. As each of these optical ranges has both advantages and disadvantages, it is effective to fuse information from different sensors in low visibility conditions. The result of pixel-level fusion [3] is an image, which, as a rule, carries more information than images from each of the vision channels separately [4]. However, before performing the procedure of pixel-level fusion of multispectral images from different sensors, it is necessary to first perform their geometric alignment (superimposition).

2. Related work

There are several popular strategies for estimating the parameters of the projective transformation, leading (under certain conditions) to the accuracy of superimposition of multispectral images no worse than units of pixels. Brown and Susstrunk [5] use the classical SIFT method [6] for images of visible and NIR ranges. Visilter at al. [7] apply for this purpose the methods of diffuse morphology and diffuse correlation. Efimov, Novikov, and Sablina [8] perform a search for descriptors along the contours. If it is required to superimpose images of distant objects, then the pixel coordinates of pairs of correspondences can be determined even in manual mode [9-12]. In the general case, there are several

GraphiCon 2022: 32nd International Conference on Computer Graphics and Vision, September 19-22, 2022, Ryazan State Radio Engineering University named after V.F. Utkin, Ryazan, Russia
EMAIL: kholopov.i.s@rsreu.ru (I. Kholopov); i.a.kudinov@yandex.ru (I. Kudinov); nikiforov.m.b@evm.rsreu.ru (M. Nikiforov)
ORCID: 0000-0001-5220-0811 (I. Kholopov); 0000-0003-1795-097X (I. Kudinov); 0000-0002-4796-0776 (M. Nikiforov)

quadruples of pairs of correspondences, that provide optimal (in the sense of the minimum mean squared error) geometric alignment [11].

Taking into account that under poor visibility conditions images in one or even several EVS technical vision channels may in principle not contain informative objects (see, for example, Bondarenko [13] – frames of visible and LWIR channels in dense drizzle), the authors believe that at a priori uncertainty about the shooting conditions, the most robust approach to superimposition is based on the preliminary photogrammetric calibration of the EVS cameras [14]. For simultaneous calibration of all EVS cameras, a universal test object (UTO) is needed, which ensures the forming of a high-contrast image by cameras of all spectral ranges. UTO assumes the presence of a heater and structural elements that provide thermal contrast [15-21]. Such elements of UTO can be:

- plates, made of optical glass [15], which does not transmit IR radiation;
- masks (glass, ceramic) placed in front of the heating element that does not transmit IR radiation [16];
- coatings of film or printing ink of dark color that provide better radiation of IR waves [17-19];
- Peltier semiconductor elements [20];
- halogen lamps [21].

In this paper, we will consider two options for the implementation of UTO, as well as the design of a device for automated calibration.

3. Examples of planar universal test objects for camera calibration

3.1. The chessboard-like planar universal test object

The design of a planar UTO of this type is considered in detail in [14]. It consists of the light aluminum plate 1, electric heating element 2, squares from vinyl dark film 3, the thermostat 4,and stiffening ribs 5 (are mounted on reverse side) for good flatness (Figure 1).

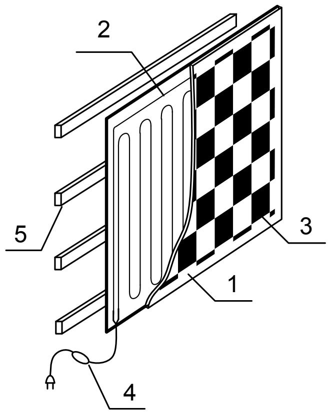

Figure 1: The design of planar UTO

Cells, covered with a dark film, on a frame from a thermal camera (MWIR, LWIR) form images with high brightness; not closed –with low brightness. Therefore, in order to the UTO images on the frames from the thermal cameras to coincide with the frames of the cameras fixing reflected light (visible, NIR, and SWIR), the frame from the thermal camera must be inverted before calibration. Figure 2 demonstrates that this type of UTO makes it possible to form visible, SWIR and LWIR frames with high contrast for subsequent use in the calibration procedure according to Zhang's method [22].

The disadvantage of this calibration UTO is the placement of the electric heating element directly on the plate with a "chessboard" pattern. A limited length of the cable that feeds the electric heater, leads to a limited range of movement of the test object during calibration.

a *b* *c*

Figure 2: Images of planar UTO: *a* – visible, *b* – LWIR, *c* – SWIR

3.2. The Chessboard-like planar universal test object with heating dock station

In UTO of this type (see Figure 3) the heating element is not connected to the aluminum board. In this case, to ensure uniform heating of the movable part of the test object, it is advisable to use a planar IR electric heater with a length and width not less than the length and width of the movable part. The design of a planar UTO of this type consists of the light aluminum plate 1, squares from vinyl dark film 2, and the thermostat 4 too, and electric IR dock station like heating element 3.

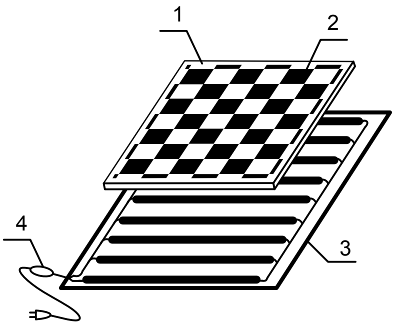

Figure 3: The design of planar UTO with IR heating dock station

For an aluminum plate with a size of 500×500×6 mm, the time interval from the moment of warming up to the operating temperature until the moment the thermal contrast drops below the threshold value of 0.2 is 5-6 minutes. Figure 4 shows images of a heated aluminum plate obtained using a measuring thermal camera Testo 875 after a five-minute warm-up. Wireless UTO provides greater freedom of movement.

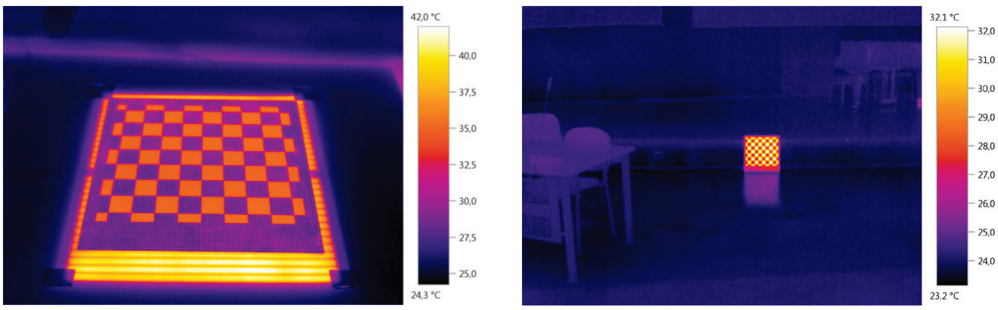

a *b*

Figure 4: Images of the removable part of UTO: *a* – distance from thermal camera to UTO is 0.6 m (UTO lies on dock station), *b* – distance from thermal camera to UTO is 9.5 m

4. Design of device for automated EVS cameras calibration

The design of the proposed device for automated calibration is shown in Figure 5. It consists of a base 1 (for example, a honeycomb optical plate), on which motorized mechanisms are rigidly fixed to ensure the movement of the camera (or module with several EVS cameras) 2 along three linear (depth, horizontal, and vertical) and three angular (yaw, elevation, and roll) coordinates – linear motorized translators (MT) 3, 4 and 5 and motorized rotation stages (MRS) 6, 7 and 8 respectively. Camera 2 is attached to the MRS using a special bracket 9. On opposite sides of base 1, a universal test object 10 and at least one light source 11 are placed. To protect the user's eyes from the radiation of the light source 11, an opaque screen 12 is fixed on the base 1 (for clarity, only its left and rear walls are shown in Figure 5 and the front and right walls, as well as the cover, are not shown). To automate the change of shooting angles, issuing commands for capturing a frame and saving frames with images of the UTO, a power supply and control module 13 is used. Commands and supply voltages from it are transmitted to camera 2, MTs 3-5 and MRSs 6-8 via cables 14, 15-17 and 18-20, respectively. Cable 21 is optional – for powering the electric heater, if UTO 10 is not wireless.

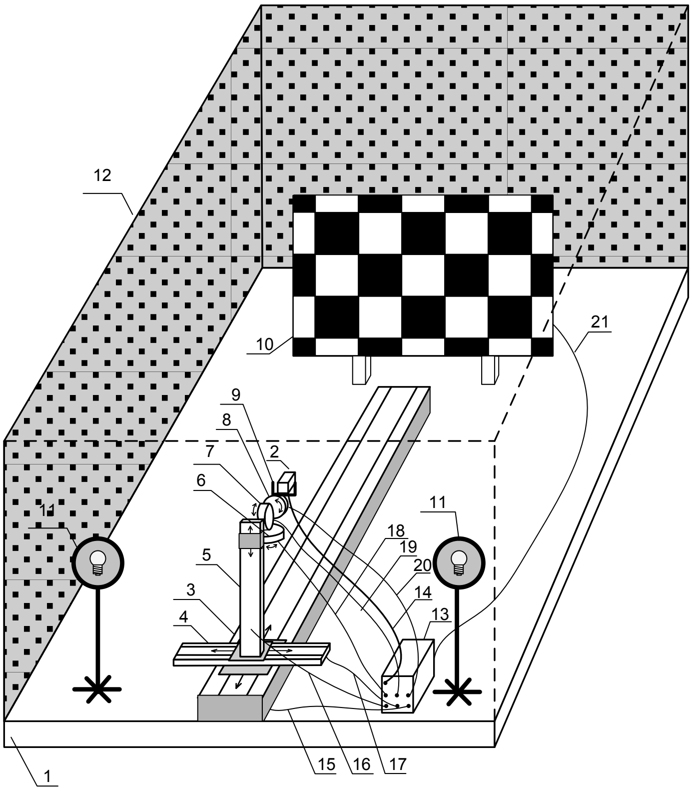

Figure 5: The design of device for automated cameras calibration: back view

The device for automated cameras calibration is used as follows. To calibrate multispectral EVS cameras using MTs 3-5 MRSs 6-8, on commands from the power supply and control device 13, the angular and spatial position of the calibrated cameras is changed so that the UTO 10 is observed from different angles, and its image is completely into the frames of cameras and at the same time amounted to at least 50% of the frame area.

By changing the shooting angles in such a way that the images of UTO are located both in the central part of the camera frames and along the edges, a series of frames taken from different angles are saved. At each shooting angle (the recommended number of angles is at least 15), pixel coordinates of UTO reference points are automatically allocated in each frame, which is then used in the calibration algorithm, for example, according to [22].

An example of the device design is shown in Figure 6.

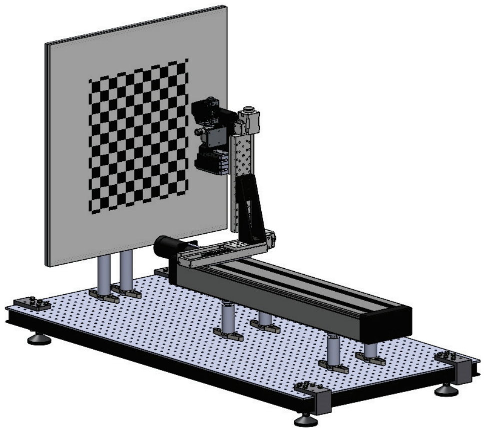

Figure 6: The part of device for automated cameras calibration: Standa [23] opto-mechanical products are used.

The evaluation of the homography matrix based on the results of preliminary photogrammetric calibration is determined by the expression [24]:

$$\mathbf{H}_{ij} = \mathbf{K}_i[\mathbf{R}_{ij} - \mathbf{t}_{ij}\mathbf{n}^{\mathrm{T}}/d]\mathbf{K}_j^{-1}, \quad (1)$$

where $\mathbf{K}_i$ and $\mathbf{K}_j$ are intrinsic matrices, $i \neq j$, $i, j = 1..N_{\mathrm{cam}}$, $\mathbf{R}_{ij}$ and $\mathbf{t}_{ij}$ are rotation matrix and translation vector of j-th camera coordinate system relative to i-th camera coordinate system respectively, d is the length of the perpendicular to the shooting plane with the normal $\mathbf{n}$ relative to the coordinate system of the reference camera (number i in this case), N_{cam} is a number of EVS cameras. In $d >> \|\mathbf{t}_{ij}\|$, then (1) is converted to the form [2]:

$$\mathbf{H}_{ij} \approx \mathbf{K}_i\mathbf{R}_{ij}\mathbf{K}_j^{-1}. \quad (2)$$

The homography matrix determines the relationship between homogeneous pixel coordinates of objects on camera frames:

$$\mathbf{x}_i = \mathbf{H}_{ij}\mathbf{x}_j. \quad (3)$$

5. Results and Discussion

We have performed an experiment to superimpose images from two cameras with different fields of view (FoV): the visible range and LWIR (Figure 7). For the wireless UTO (Figure 3), we received 15 images, according to which we estimated the matrices of the internal and external parameters of these cameras [22]:

$$\mathbf{K}_{\mathrm{vis}} = \begin{bmatrix} 2045.5 & 383.1 & 0 \\ 0 & 2181.0 & 379.2 \\ 0 & 0 & 1 \end{bmatrix}, \ \mathbf{K}_{\mathrm{LWIR}} = \begin{bmatrix} 1637.1 & 371.0 & 0 \\ 0 & 1640.1 & 303.00 \\ 0 & 0 & 1 \end{bmatrix},$$

$$\mathbf{R} = \begin{bmatrix} 0.9999 & -0.008 & -0.004 \\ 0.008 & 0.9998 & -0.0185 \\ 0.004 & 0.018 & 0.9998 \end{bmatrix}, \ \mathbf{t} = \begin{bmatrix} 293.40 \\ 70.73 \\ 75.07 \end{bmatrix},$$

and estimated radial distortion coefficients:

$$\mathbf{d}_{\mathrm{vis}} = [0.223, 0.075]^{\mathrm{T}}, \ \mathbf{d}_{\mathrm{LWIR}} = [-0.007, -2.897]^{\mathrm{T}}.$$

Since the LWIR image had a larger FOV, it was chosen as the base one. For both images, a radial distortion compensation procedure was performed [24]. The image of the visible range after performing a projective transformation with the matrix $\mathbf{H}$, calculated according to (2), is superimposed on the base image using alpha blending with a parameter $\alpha = 0.5$.

As can be seen from the fusion result (Figure 7, *c*), the superimposition according to (2) with the results of pre-calibration in the far zone (the distance to buildings on Figure 7 is greater than 300 m) provides an error of no more than 2-3 pixels (see, for example, images of window openings and a billboard in the lower right frame corner).


a *b*

c

Figure 7: Results of superimposition: *a* – visible, *b* – LWIR, *c* – fusion result

6. Conclusion

The considered designs of universal test objects make it possible to successfully calibrate cameras of different spectral ranges: visible, NIR, SWIR, MWIR, and LWIR. Based on the results of such a calibration, an superimposition error of the order of units of pixels is provided.

7. Acknowledgements

The authors express gratitude to Maxim A. Bondarenko for the opportunity to shoot the wireless test object with the Testo 875 thermal measuring camera.

The work was performed as part of the state assignment of the Ministry of Science and Higher Education of the Russian Federation (FSSN-2020-0003).

8. References

[1] C. Spitzer, U. Ferrell, T. Ferrell (Ed.), Digital Avionics Handbook, CRC Press, 2015. doi: 10.1201/b17545.

[2] J.M. Lloyd, Thermal Imaging Systems, New York, Springer Science + Business Media, LLC, 1975. doi: 10.1007/978-1-4899-1182-7.

[3] S. Li, X. Kang, L. Fang, J. Hu, H. Yin, Pixel-level image fusion: a survey of the state of the art, Inf. Fusion 33 (2017), 100–112. doi: 10.1016/j.inffus.2016.05.004.

[4] O. Vygolov, S. Zheltov, Enhanced, synthetic and combined vision technologies for civil aviation, Intell. Syst. Ref. Libr. 75 (2015) 201–230. doi: 10.1007/978-3-319-11430-9_8.

[5] M. Brown, S. Susstrunk. Multi-spectral SIFT for scene category recognition, in: Proc. IEEE Conf. on Computer Vision and Pattern Recognition (CVPR'11), 2011. doi: 10.1109/CVPR.2011.5995637.
[6] D. G. Lowe, Distinctive Image Features from Scale-Invariant Keypoints, Int. J. of Comp. Vis. 60 (2004) 91–110. doi: 10.1023/B:VISI.0000029664.99615.94.
[7] Yu. V. Vizilter, V. S. Gorbatsevich, A. Yu. Rubis, O. V. Vygolov, Image shape matching using diffusion morphology and diffusion correlation, Computer Optics 39 (2015) 267–274. doi: 10.18287/0134-2452-2015-39-2-265-274.
[8] A. I. Efimov, A. I. Novikov, V. A. Sablina, Image superimposition technique in computer vision systems using contour analysis methods, in: Proc. 5th Mediterranean Conf. on Embedded Computing (MECO), 2016, pp. 132–136. doi: 10.1109/MECO.2016.7525721.
[9] B. A. Alpatov, P. V. Babayan, Electronic image adjustment in multispectral observation [in Russian], Digital Signal Processing 1 (2003) 24–26.
[10] U. Bhosle, S. D. Roy, S. Chaudhuri, Multispectral panoramic mosaicing, Pattern Recognition Letters 26 (2005) 471–482. doi: 10.1016/j.patrec.2004.08.007.
[11] A. I. Efimov, A. I. Novikov, An algorithm for multistage projective transformation adjustment for image superimposition, Computer Optics 40 (2016) 258–265. doi: 10.18287/2412-6179-2016-40-2-258-265.
[12] Patent RU 2705423, The method of combining simultaneously obtained images from matrix photodetectors of different spectral ranges [in Russian] / M. A. Bondarenko, A. V. Bondarenko, K. A. Yadchuk,M. G. Knyazev, I. V. Dokuchaev, date of patent: 07.11.2019.
[13] A. Bondarenko, M. Bondarenko, Hardware-software implementation of the multispectral enhanced vision system [in Russian], Modern electronics 1 (2017) 32–37.
[14] A. I. Efimov, I. A. Kudinov, O. V. Melnik, M. B. Nikiforov, I. S. Kholopov, Digital multispectral images superimposition based on preliminary calibration or contour analysis: advantages and disadvantages, in: Proc. ELEKTRO Conf., Taormina, Italy, 2020, pp. 1-6. doi: 10.1109/ELEKTRO49696.2020.9130339.
[15] Patent CN 204287725, Device employing checkerboard for calibrating visible light camera and thermal infrared imager camera [in Chinese] / D. Ming, W. Zhang, H. Zhong, H. Qi, S. Di, C. Yongfei, J. Xudong, C. Guojun, L. Fengyang, H. Ting, W. Hui, date of patent: 22.04.2015.
[16] S. Vidas, R. Lakemond, S. Denman, C. Fookes, S. Sridharan, T. Wark, A mask-based approach for the geometric calibration of thermal-infrared cameras, IEEE Trans. on Instrumentation and Measurement 61 (2012) 1625–1635. doi: 10.1109/TIM.2012.2182851.
[17] A. Choinowski, D. Dahlke, I. Ernst, S. Pless, Automatic calibration and co-registration for a stereo camera system and a thermal imaging sensor using a chessboard, in: Proc. Int. Archives of the Photogrammetry, Remote Sensing and Spatial Information Sciences, Enschede, 2019, pp. 1631–1635. doi: 10.5194/isprs-archives-XLII-2-W13-1631-2019.
[18] A. P. Alekseev, E. V. Goshin, N. S. Davydov, N. A. Ivliev, A. V. Nikonorov, Visual-inertial odometry algorithms on the base of thermal camera, CEUR Workshop Proc. 2416 (2019) 183–188. doi: 10.18287/1613-0073-2019-2416-183-188.
[19] L. St-Laurent, M. Mikhnevich, A. Bubel, D. Prevost, Passive calibration board for alignment of VIS-NIR, SWIR and LWIR images, Quantitative InfraRed Thermography J. 14 (2017) 193–205. doi: 10.21611/qirt.2016.124.
[20] Y. Chen, F.-y. Huang, F. m. Shi, B.-q. Liu, Plane chessboard-based calibration method for a LWIR ultra-wide-angle camera, Applied Optics 58 (2019) 744. doi: 10.1364/AO.58.000744.
[21] Y. W. K. Zoetgnande, A. J. Fougeres, G. Cormier, J. L. Dillenseger, Robust low-resolution thermal stereo camera calibration, in: Proc. 11th Int. Conf. on Machine Vision, Munich, 2018. doi: 10.1117/12.2523440.
[22] Z. Zhang, A flexible new technique for camera calibration, IEEE Trans. on Pattern Analysis and Machine Intelligence 22 (2000) 1330–1344. doi: 10.1109/34.888718.
[23] Standa opto-mechanical products, URL: https://www.standa.lt/products (time to request: 01.02.2022).
[24] R. Hartley, A. Zisserman, Multiple view geometry in computer vision, 2nd ed., Cambridge University Press, 2003. doi: 10.1017/CBO9780511811685.